Electrical Materials and Applications

WILEY

国家电网 STATE GRID 国网智能电网研究院有限公司 STATE GRID SMART GRID RESEARCH INSTITUTE CO.,LTD.

The Institution of Engineering and Technology

ORIGINAL RESEARCH OPEN ACCESS

Simulation and Verification of Magnetic Hysteresis Characteristics of Electrical Steel Sheets Based on the J-A Model

Mengxue Lu[1] | Chengxu He[2,3] | Gang Lei[4] | Nana Duan[1]

[1]School of Electrical Engineering, Xi'an Jiaotong University, Xi'an, China | [2]Institute of New Electrical Material, China Electric Power Research Institute, Beijing, China | [3]State Key Laboratory of Advanced Power Transmission Technology, Beijing, China | [4]School of Electrial and Data Engineering, University of Technology Sydney, Sydney, Australia

Correspondence: Nana Duan (duannana@xjtu.edu.cn)

Received: 26 June 2025 | **Revised:** 25 August 2025 | **Accepted:** 12 September 2025

Funding: This work was supported by the National Natural Science Foundation of China (52077161).

Keywords: hysteresis model | J-A model | least squares method | PSO algorithm

ABSTRACT

Electrical steel sheets, as core components of electromagnetic equipment, are indispensable in modern power equipment. The magnetic hysteresis characteristics of electrical steel sheets have a significant impact on key performance indicators such as energy efficiency and lifespan of electromagnetic equipment. Accurately simulating the magnetic hysteresis characteristics of electrical steel sheets plays a crucial role in the design and optimisation of electromagnetic equipment. This paper analyses the classical J-A model and the inverse J-A model. Three parameter identification methods—least squares method based on the partial difference method, least squares method based on the ordinary differential method and particle swarm optimisation algorithm—are used to identify the model parameters. After comparing the results with experimental data, it is found that each algorithm has its advantages. At $B_{max} = 1.7$ T, the simulation results based on the differential method of least squares are almost identical to the experimental results. However, overall, the PSO algorithm is more universal.

1 | Introduction

Electrical steel sheets are a critical material in power equipment, offering advantages over other soft magnetic materials, such as lower cost, mature processing technology and high magnetic induction [1, 2]. Electrical steel sheets are primarily used to manufacture cores and are widely applied in electromagnetic devices such as transformers, motors and reactors, making them an irreplaceable material in modern power equipment [3–5]. Electrical steel sheets exhibit hysteresis characteristics, which can affect core indicators such as energy efficiency, thermal stability, structural vibrations and lifespan of electromagnetic devices [6, 7]. Accurately simulating the hysteresis characteristics of electrical steel sheets is not only the foundation for efficient design but also an indispensable support method for achieving digitalisation and intelligent electrification of equipment [8–11].

Classic hysteresis models include the Preisach model [12], the Jiles–Atherton (J-A) model [13], the Stoner–Wohlfarth model [14], the E&S model [15] and the hybrid hysteresis model [16]. Among these, the J-A model has the advantages of clear physical significance for its parameters, fewer parameters, high-computational efficiency, ease of fitting and modelling and high scalability. It is widely used in the field of magnetic characteristic simulation research. The simulation accuracy of the hysteresis loop is determined by the parameters of the J-A model, so how to accurately simulate these parameters has become a key issue. Current research on the J-A model primarily focuses on two aspects [17, 18]: modifications and

improvements to the traditional J-A model and parameter identification algorithms for the J-A model. The authors in ref. [19] proposed a hybrid algorithm that combines simulated annealing and particle swarm optimisation (PSO), integrating the advantages of both algorithms to improve the speed and effectiveness of parameter identification in engineering applications. The authors in ref, [20] introduced R-L type fractional derivatives to improve the J-A model expression and applied the annealing algorithm for parameter identification. A comparison with experimental data showed that the average absolute error of the loss prediction was 7.35%. The authors in ref. [21] addressed the low accuracy and long computational time of existing parameter identification methods for the J-A model by using an improved vulture algorithm for parameter identification, effectively improving the convergence speed and accuracy of the identification process.

The working conditions of modern electromagnetic devices are becoming increasingly complex, and it is currently impossible to find a universal parameter identification method. Therefore, model corrections and improvements to parameter identification methods must be made for specific working conditions and material characteristics. In this paper, a 0.15-mm oriented silicon steel is used, and three parameter identification methods are applied to simulate its hysteresis characteristics: the least squares method based on the finite difference method, the least squares method based on the differential method and the particle swarm optimisation algorithm based on the inverse J-A model. The accuracy of these methods is compared. The results show that different parameter identification methods have significant differences under different working conditions, and there is an optimal parameter identification method for a specific working condition.

2 | Jiles–Atherton Model

The Jiles–Atherton (J-A) model [22, 23] was developed based on the theory of magnetic domains and the principle of minimum energy, aiming to provide a physically interpretable explanation of the hysteresis phenomenon in ferromagnetic materials. Starting from the microstructure of ferromagnetic materials, Jiles and Atherton established a model that not only possesses a solid physical foundation but also offers mathematical tractability, thereby overcoming many of the limitations associated with traditional models.

2.1 | Classical J-A Model

In the classical J-A model, the magnetisation M is composed of two components: the reversible component M_{rev} and the irreversible component M_{irr}, as shown in Equations (1) and (2).

$$M = M_{\text{irr}} + M_{\text{rev}} \tag{1}$$

$$M_{\text{rev}} = c(M_{\text{an}} - M_{\text{irr}}) \tag{2}$$

In Equation (1), M_{rev} is the reversible magnetisation component, generated by the elastic deformation of domain walls, whereas M_{irr} is the irreversible magnetisation component, caused by domain wall pinning. In Equation (2), c is the reversible magnetisation coefficient, and M_{an} is the hysteretic-free magnetisation.

Based on Langevin paramagnetic theory, an analytical expression for the hysteretic-free magnetisation can be obtained. It was developed on the basis of paramagnetic materials and applied to ferromagnetic materials. The classical Langevin function is shown in Equation (3).

$$\begin{cases} M_{\text{an}}(H_a) = M_{\text{sat}}\left[\coth\left(\dfrac{H_a}{a}\right) - \dfrac{a}{H_a}\right] \\ H_a = H + \alpha M \end{cases} \tag{3}$$

In Equation (3), H_a is the applied magnetic field strength, $a = k_B T/\mu_0 m$, where k_B is the Boltzmann constant, T is the absolute temperature of the material, μ_0 is the permeability of free space and m is the magnetic moment of each dipole in the material. In the J-A model, H_e is used to replace H_a, where H_e represents the effective magnetic field strength; M_{sat}, abbreviated as M_s, represents the saturation magnetisation.

From the theoretical analysis of hysteretic-free magnetisation, irreversible magnetisation and reversible magnetisation in Equations (1–3), the energy balance equation for magnetic materials can be derived, as shown in Equation (4)

$$\mu_0 \int M dH_e = \underbrace{\mu_0 \int M_{\text{an}} dH_e}_{A} - \underbrace{\mu_0 k\delta \int \frac{dM_{\text{irr}}}{dH_e} dH_e}_{B} \tag{4}$$

The left-hand side of the differential equation shown in Equation (4) represents the magnetic energy in the magnetic material. Term A on the right-hand side represents the energy supplied by the external excitation magnetic field, and term B represents the energy consumed by irreversible magnetisation. k denotes the pinning effect, and δ is the sign function with respect to the magnetic field strength H, where $\delta = 1$ when $dH/dt > 0$, and $\delta = -1$ when $dH/dt < 0$.

According to Equations (1–4), the differential equation between the magnetisation M and the magnetic field strength H can be derived, namely the J-A direct hysteresis model, as shown in Equation (5).

$$\frac{dM}{dH} = \frac{(1-c)(M_{\text{an}} - M) + c\delta k \frac{dM_{\text{an}}}{dH}}{\delta k - \alpha(1-c)(M_{\text{an}} - M)} \tag{5}$$

2.2 | Inverse J-A Model

Considering that in practical engineering applications, the magnetic field strength H is difficult to obtain and its measured values are easily distorted, the magnetic flux density B is chosen as the input variable. The relationship between magnetic flux density B and magnetic field strength H is given by Equation (6):

$$B = \mu_0(M + H) \tag{6}$$

Substituting Equation (6) into Equation (3) gives Equation (7):

$$H_e = \frac{B}{\mu_0} - (1-\alpha)M \tag{7}$$

Substituting Equation (7) into Equation (4) gives Equation (8).

$$\frac{dM}{dB} = \frac{\delta_M(1-c)(M_{an}-M_s) + ck\delta\frac{dM_{an}}{dH_e}}{\mu_0\left[(1-\alpha)\left(\delta_M(1-c)(M_{an}-M_s) + ck\delta\frac{dM_{an}}{dH_e}\right) + k\delta\right]} \tag{8}$$

In Equation (8), δ_M is a factor used to prevent nonphysical behaviour [24].

$$\delta_M = \begin{cases} 1, \text{sign}(M_{an}-M)\cdot\text{sign}(dH/dt) \geq 0 \\ 0, \text{sign}(M_{an}-M)\cdot\text{sign}(dH/dt) < 0 \end{cases} \tag{9}$$

Among Equations (2–9), the parameters c, M_s, a, α and k are all critical factors affecting the accuracy of the J-A model. Any change in these parameters will influence the shape of the hysteresis loop.

2.3 | Model Parameter Calculation Method

The parameters in the model can be determined using experimental data. Once the field values, the differential susceptibility at the initial point, the tips of the hysteresis loop and the remanent induction and coercive field are known, the parameters of the J-A model can be calculated at these specific points, as shown in Figure 1.

According to the physical meanings of the parameters in the model, the easiest parameter to obtain is M_s, which can be found in manuals or measured by placing the material in a sufficiently strong magnetic field and measuring its magnetic flux density B or magnetisation M with a coil and then calculating M_s.

In the model, the parameter c determines the reversible magnetisation component caused by reversible bending and translation of domain walls. At the beginning of the magnetisation curve, it can be expressed as Equation (10).

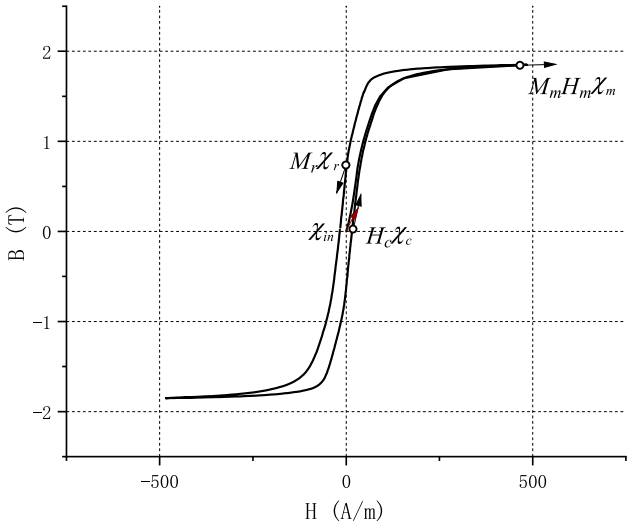

FIGURE 1 | Special points for determining model parameters.

$$\chi_{in} = \left.\frac{dM}{dH}\right|_{H=0} = c\frac{dM_{an}}{dH} \tag{10}$$

At low magnetic fields, the hysteretic-free magnetisation can be expressed as Equation (11).

$$M_{an} = M_s\frac{H}{3a} \tag{11}$$

Therefore, the parameter c can be obtained from Equation (12).

$$c = \frac{3a\chi_{in}}{M_s} \tag{12}$$

At this point, assuming that a is known and M_s is obtained from experimental data, the parameter c can be calculated using Equation (12).

The parameter α can be obtained at the remanent magnetisation M_r, where $\delta = 1$, $H = 0$ and $M = M_r$.

$$M_r = M_{an}(M_r) + \frac{k}{\frac{\alpha}{1-c} + \frac{1}{\chi_r - c\frac{dM_{an}(M_r)}{dH}}} \tag{13}$$

An initial value is assumed for parameters a and k. By combining the previously calculated parameter c, and using Equations (3) and (13), the parameter α can be obtained. Substituting parameter α into Equation (14) will allow for the calculation of parameter a.

$$a = \frac{M_s}{3}\left(\frac{1}{\chi_{in}} + \alpha\right) \tag{14}$$

Using the parameters α, c, M_s and the updated parameter a, the parameter k can be calculated at the coercive force point. At this point, $H = H_c$, $M = 0$.

$$k = \frac{M_{an}(H_c)}{1-c}\left[\alpha + \frac{1-c}{\chi_c - c\frac{dM_{an}(H_c)}{dH}}\right] \tag{15}$$

Parameters k can be obtained from Equations (3) and (15).

Thus, the preliminary calculation of all parameters in the J-A model is completed, providing initial values that are close to the target solution. Next, a series of parameter identification methods can be used to simulate the hysteresis characteristics of electrical steel sheets.

3 | Parameter Identification Method

3.1 | Least Squares Fitting

Since the J-A model is expressed as a differential equation, there are two numerical methods for solving it: ordinary differential equations (ODE) and partial differential equations

(PDE). In this study, MATLAB is used to solve the equations. Two numerical approaches are implemented to solve the J-A model: specifically, the Runge–Kutta method [25, 26] and the finite difference method [27]. In the following sections, these two methods will be referred to as ODE and PDE, respectively.

The fourth-order Runge–Kutta solution is shown in Equation (16).

$$\begin{cases} k_1 = f(t_n, y_n) \\ k_2 = f\left(t_n + \frac{h}{2}, y_n + \frac{h}{2}k_1\right) \\ k_3 = f\left(t_n + \frac{h}{2}, y_n + \frac{h}{2}k_2\right) \\ k_4 = f(t_n + h, y_n + hk_3) \\ y_{n+1} = y_n + \frac{h}{6}(k_1 + 2k_2 + 2k_3 + k_4) \end{cases} \tag{16}$$

For the finite difference method, the backward difference scheme is used, and its expression is given in Equation (17).

$$\begin{cases} u = u(x) \\ x_{i+1} = x_i + h \\ u_i = u_{i-1} + h \times du/dx \end{cases} \tag{17}$$

After implementing both solution methods, the least squares method [28, 29] is used for parameter fitting. By setting upper and lower bounds for the parameters to be identified and using the initially calculated J-A model parameters, an iterative computation of the parameters can be performed.

3.2 | PSO Algorithm

The particle swarm optimisation (PSO) algorithm [30, 31] is a type of evolutionary computation technique, inspired by the social behaviour of birds foraging for food. The basic idea of PSO is to find the optimal solution through cooperation and information sharing among individuals in a population. Each candidate solution is imagined as a bird, referred to as a "particle." All particles search in an N-dimensional space, and each particle's quality is evaluated by a fitness value determined by the objective function.

Each particle has a memory to record the best position it has found so far. Additionally, each particle has a velocity, which determines how it moves through the search space. The velocity is dynamically adjusted based on both the particle's own experience and the experience of its companions. The velocity of each particle is updated using Equation (18), and the position is updated using Equation (19).

$$v_i = w \times v_i + c_1 \times rand() \times (gbest_i - x_i) + c_2 \times rand() \times (zbest_i - x_i) \tag{18}$$

$$x_i = x_i + v_i \tag{19}$$

In these equations, w is the inertia weight, c_1 is the cognitive acceleration coefficient and c_2 is the social acceleration coefficient. In Equation (18), $w \times v_i$ represents the inertia component, reflecting the particle's tendency to maintain its current motion; $c_1 \times rand()$ is the cognitive component, representing the particle's tendency to adjust its velocity based on its own best experience; and $c_2 \times rand() \times (zbest_i - x_i)$ is the social component, reflecting the particle's tendency to approach the best experience found by the swarm.

In the context of inverse J-A model parameter estimation, each particle represents five unknown parameters (M_s, a, α, c, k). Equation (20) is used as the fitness function.

$$\text{Fitness}(x) = \sqrt{\frac{1}{N}\sum_{i=1}^{N}\left(H_{\text{real},i} - H_{\text{model},i}\right)^2} \tag{20}$$

In this equation, N is the number of sample points, H_{real} is the measured magnetic field strength and H_{model} is the computed magnetic field strength from the simulation.

The flowchart of the PSO algorithm used in this study is shown in Figure 2.

4 | Conclusion

To validate the effectiveness of the parameter identification algorithms proposed in this paper when applied to J-A model identification, an MPG200D arbitrary waveform magnetic field excitation measurement system was used. The measurements were conducted under environmental conditions of 23°C ± 5°C and relative humidity of 50% ± 15%. Parameter identification

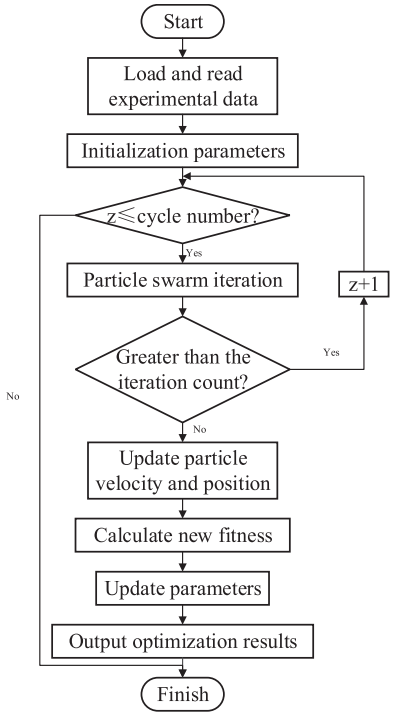

FIGURE 2 | Flowchart of the PSO algorithm.

was then carried out based on the experimentally measured hysteresis loops for two magnetic flux densities: B_{max} = 1.7 T and B_{max} = 1.85 T. The performance table of the experimental samples is shown in Table 1.

The number of cycles in the particle swarm algorithm has a significant impact on the fitting results. When the number of cycles is too small, convergence is insufficient, leading to large identification errors and unstable results. When the number of cycles is too large, convergence stagnates, resulting in wasted computational resources and an increased risk of overfitting, which can negatively affect fitting accuracy. Therefore, it is necessary to determine an appropriate number of cycles to improve identification accuracy and obtain stable results. Table 2 shows the fitting results and experimental data errors under different cycle numbers. The number of cycles is consistent with the description in Table 2 and the Figure 2 and is represented by z.

Table 2 shows the area and relative error of the hysteresis loop obtained from the experiment and the hysteresis loop obtained from the fitting parameters. It can be seen that the calculation law is consistent with the law proposed in the above text. In this paper, the number of cycles is selected as 7.

For B_{max} = 1.85 T, the parameter identification results using three methods—least squares based on ordinary differential equations, least squares based on partial differential equations and the PSO algorithm—are shown in Table 3.

The corresponding hysteresis loop comparison based on the results in Table 1 is shown in Figure 3.

Figure 4 shows the hysteresis curve generated based on parameter identification results for B_{max} = 1.7 T.

As shown in Figures 3 and 4, the fitting results of the three parameter identification methods are quite satisfactory. For the accuracy of the quantitative analysis algorithm, the relative error of parameter identification at B_{max} = 1.7 T and B_{max} = 1.85 T is shown in Table 4.

As shown in Table 4, when the B_{max} = 1.7 T, all three algorithms exhibit excellent computational accuracy. Among them, the least squares fitting algorithm based on ordinary differential equations demonstrates a significant advantage in accuracy. When B_{max} = 1.85 T, the PSO algorithm shows a clear advantage in accuracy. However, compared to the case where B_{max} = 1.7 T,

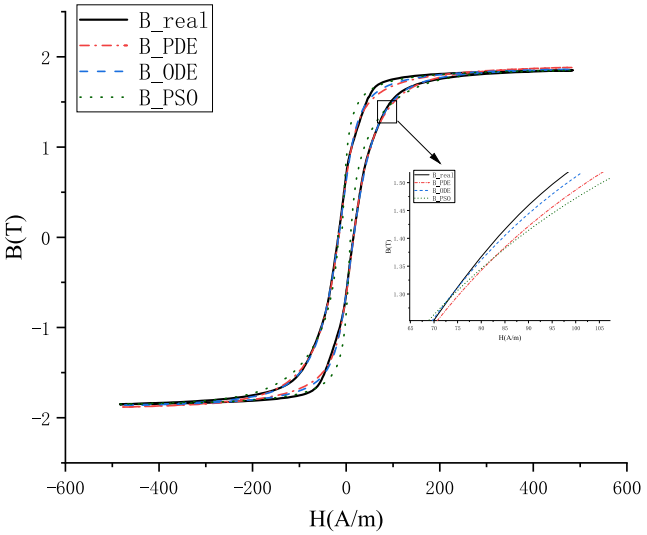

FIGURE 3 | Comparison of hysteresis curves generated using measured data and the parameters identified by each algorithm. (B_{max} = 1.85 T).

TABLE 1 | Experimental sample performance table.

Grade	Nominal thickness/mm	Maximum specific loss $P_{1.5/400}$ (W/kg)	Minimum magnetic polarisation strength (50 Hz/60 Hz) J_{800}	Minimum stacking coefficient
15SQF1250	0.15	12.5	1.83	0.940

TABLE 2 | Computational error of the particle swarm algorithm at different numbers of cycles.

	Experiment	z = 5	z = 6	z = 7	z = 8	z = 9
Hysteresis loss (B_{max} = 1.85 T) J/m^3	166.8507	208.8194	227.7325	176.9003	226.9904	217.6987
Relative error	—	25.15%	36.49%	6.02%	36.04%	30.48%
Hysteresis loss (B_{max} = 1.7 T) J/m^3	98.6858	97.1886	97.4713	97.6036	96.4174	97.4804
Relative error	—	1.52%	1.23%	1.10%	2.30%	1.22%

TABLE 3 | Parameter identification results of each algorithm.

Parameters	M_s	α	a	k	c
Experiment	1,472,000	1.393×10^{-5}	38.045	12.104	0.353
PDE_Lsqcurvefit	1,551,694	1.555×10^{-5}	17.4155	14.236	0.699
ODE_Lsqcurvefit	1,523,424	2.723×10^{-6}	13.1825	19.935	0.380
PSO	1,507,419	1.533×10^{-5}	11.0778	23.346	0.6782

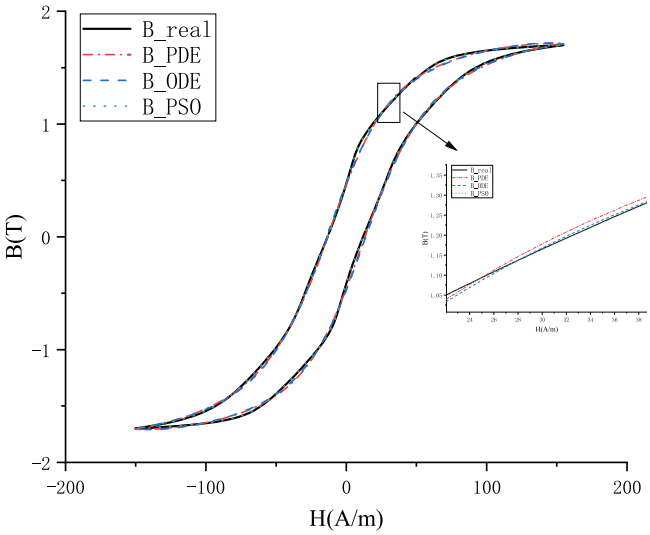

FIGURE 4 | Comparison of hysteresis curves generated using measured data and the parameters identified by each algorithm. (B_{max} = 1.7 T).

TABLE 4 | Relative errors of parameter identification by each algorithm.

	FDE_Lsqcurvefit (%)	ODE_Lsqcurvefit (%)	PSO (%)
B_{max} = 1.7 T	0.71	0.06	1.10
B_{max} = 1.85 T	12.39	8.08	6.02

the computational accuracy of all three algorithms decreases, which may be due to the relatively low fitting accuracy at the knee point of the hysteresis loop.

Overall, the PSO algorithm demonstrates greater universality. In the future, the model will be optimised based on the magnetisation mechanism of oriented silicon steel to improve fitting accuracy at the knee point of the hysteresis loop. A detailed analysis of the causes of errors will be conducted, and the parameter identification algorithm will be further refined to achieve higher computational accuracy.

Author Contributions

Mengxue Lu: writing – original draft, validation, methodology, data curation. **Chengxu He:** methodology. **Gang Lei:** writing – review and editing. **Nana Duan:** writing – review and editing.

Conflicts of Interest

The authors declare no conflicts of interest.

Data Availability Statement

Research data are not shared.

References

1. R. Liu, Y. Zeng, A. Hu, and B. Tang, "Modified Static Hysteresis Simulation Method for Silicon Steel Core of Electrical Equipment," *Electric Power* 58, no. 7 (2025): 137–146, http://kns.cnki.net/kcms/detail/11.3265.tm.20250510.2042.002.html.

2. X. Lin, H. Zhang, and Z. Liu, "Parameter Identification of J-A Hysteresis Model Based on Improved PSO With Shrinking Factor," *Journal of Electrical Engineering* 19, no. 1 (2024): 187–195, https://doi.org/10.11985/2024.01.020.

3. Z. Li, Y. Ma, A. R. Hu, L. Zeng, S. Xu, and R. Pei, "Investigation and Application of Magnetic Properties of Ultra-Thin Grain-Oriented Silicon Steel Sheets Under Multi-Physical Field Coupling," *Materials* 15, no. 23 (2022): 8522, https://doi.org/10.3390/ma15238522.

4. C. Zhang, K. Wang, C. Wang, et al., "Optimized Design of Hybrid Core for Power Transformers," *Transformer* 61, no. 10 (2024): 1–5, https://doi.org/10.19487/j.cnki.1001-8425.2024.10.010.

5. S. Imamori, S. Aihara, H. Shimoji, A. Kutsukake, and K. Hameyer, "Evaluation of Local Magnetic Degradation by Interlocking Electrical Steel Sheets for Effective Modelling of Electrical Machines," *Journal of Magnetism and Magnetic Materials* 500 (2020): 166372, https://doi.org/10.1016/j.jmmm.2019.166372.

6. S. Li, L. Chen, Z. Zhang, et al., "Loss Calculation for Laminated Cores Based on Nonlinear Complex Permeability Model," *Advanced Technology of Electrical Engineering and Energy* 42, no. 4 (2023): 68–76, https://kns.cnki.net/kcms2/article/abstract?v=djJQlkjC3sBJ0Eb1TSPZwfrqym0HcMiin22g_190xCmyGdo0xlBPnY_rLOP2IK_AtbL0bNUk2sXVgW_L6h75gjKVniUX02olwF0OpBWPsgQW3YxKGX4CYxeuh0zYGe18OXW7a0r_DoOlHQkeUUZl5s__3erMD9XZ4VoulmCeDLQ=&uniplatform=NZKPT&language=CHS.

7. T. Yamaguchi, Y. Kawase, and S. Ishimura, "Influence of Magnetic Properties of Transformer Electrical Steel Sheets on Eddy Current Loss," *Journal of the Japan Society of Applied Electromagnetics and Mechanics* 27, no. 1 (2019): 67–72, https://doi.org/10.14243/jsaem.27.67.

8. M. I. Milyaev, Y. S. Ostanin, I. N. Abdugaliyev, A. N. Solomin, C. Shumei, and Z. Chunbo, "Influence of Isothermal Treatment on Magnetic and Hysteresis Properties of Materials for Nonlinear Magnetic Systems of Hysteretic Electromechanical Energy Converters," *Bulletin of the Russian Academy of Sciences: Physics* 88, no. 11 (2024): 1747–1751, https://doi.org/10.1134/s1062873824708195.

9. Y. Zhang, X. Wu, F. Qiu, et al., "Dynamic Observation of Magnetic Domains and Hysteresis Simulation in Electrical Steel Under Magnetic-Mechanical Coupling," *High Voltage Engineering* 50, no. 10 (2024): 4429–4439, https://doi.org/10.13336/j.1003-6520.hve.20240802.

10. J. Ji, Z. Zhao, S. Zhang, et al., "Hysteresis Prediction for Nanocrystalline Materials Under High-Frequency Excitation Using Energy Model and Numerical Electromagnetic Method," *Proceedings of the CSEE* 45, no. 5 (2025): 2027–2039, https://doi.org/10.13334/j.0258-8013.pcsee.231844.

11. J. Ji and Z. Zhao, "Prediction of Hysteresis Characteristics of Amorphous Materials Based on Static Jiles–Atherton Model and Maxwell's Equation," *Journal of Magnetism and Magnetic Materials* 588, no. Part A (2023): 171460, https://doi.org/10.1016/j.jmmm.2023.171460.

12. F. Preisach, "Über die magnetische Nachwirkung," *Zeitschrift für Physik* 94, no. 5–6 (1935): 277–302, https://doi.org/10.1007/bf01349418.

13. D. Li, Y. Wu, C. Zhu, et al., "J-A Model Parameter Identification Based on Sparrow Search Algorithm and Genetic Algorithm," *High Voltage Engineering* 48, no. 10 (2022): 4181–4188, https://doi.org/10.13336/j.1003-6520.hve.20210840.

14. E. C. Stoner and E. P. Wohlfarth, "A Mechanism of Magnetic Hysteresis in Heterogeneous Alloys," *IEEE Transactions on Magnetics* 27, no. 4 (July 1991): 3475–3518, https://doi.org/10.1109/TMAG.1991.1183750.

15. M. Enokizono and N. Soda, "A New Modeling of Vector Magnetic Properties for Magnetic Field Analysis," *Studies in Applied Electromagnetics and Mechanics* 13 (1998): 418–421.

16. D. Li, Z. Qiao, N. Yang, Y. Song, and Y. Li, "Study on Vector Magnetic Properties of Magnetic Materials Using Hybrid Hysteresis Model," *CES Transactions on Electrical Machines and Systems* 3 (2019): 292–296, https://doi.org/10.30941/cestems.2019.00038.

17. R. Liu, C. Gu, J. Sun, et al., "Improved Jiles-Atherton Model for Accurate Simulation of Complex Hysteresis in Soft Magnetic Materials Under Non-Sinusoidal Excitation," *Proceedings of the CSEE* 45, no. 5 (2025): 2016–2027, https://doi.org/10.13334/j.0258-8013.pcsee.231606.

18. Y. Yu and Z. Chen, "Improved J-A Model Parameter Identification Based on Parameter *k* Calculation," *Instrumentation Technology and Sensor* 3 (2023): 98–103, https://kns.cnki.net/kcms2/article/abstract?v=djJQlkjC3sA2Q2w6UZaOnD3W1X4otXH3bz7smXX37So7cYVp-qTZ5VzDoP-ISKfc_wtwEYCk-dOyYdKjIfXdXML6sdFDzL5bdWyFmoK9npupdYTkgXZAFNjs9a1NRWyLVHVCugLXAgnNxlTHAt2Ml2-k3N0PdJRLyjMb_13-SNw=&uniplatform=NZKPT&language=CHS.

19. J. Lin, B. Yan, H. Feng, et al., "J-A Model Parameter Identification Based on PSO Improved by Simulated Annealing," *Transformer* 61, no. 2 (2024): 26–34, https://doi.org/10.19487/j.cnki.1001-8425.2024.02.009.

20. B. Chen, X. Qin, B. Tang, et al., "Dynamic J-A Model and Parameter Identification Using Fractional-Order Derivatives," *Proceedings of the CSEE* 42, no. 12 (2022): 4590–4603, https://doi.org/10.13334/j.0258-8013.pcsee.210942.

21. S. Mo, H. Yang, K. Jiang, et al., "J-A Model Parameter Identification of Transformer Based on Improved Vulture Search Algorithm," *Advanced Technology of Electrical Engineering and Energy* 41, no. 4 (2022): 67–74, https://kns.cnki.net/kcms2/article/abstract?v=djJQlkjC3sBKwhTAQ7Ulc_sfN03ricKVhzoQg59MaHqARI6Ps9xrn5io5obHIi99U-nkA0HiLmZACdLkDucjAS3hqYKFoVMCnC1QDbQ3XpjLoL_8lnrTIpWZitYJFI1CBcERBkiIqAULUN1DPfG-DRPz1V0QZwORW7KCG6smfHo=&uniplatform=NZKPT&language=CHS.

22. D. C. Jiles and D. L. Atherton, "Ferromagnetic Hysteresis," *IEEE Transactions on Magnetics* 19, no. 5 (1983): 2183–2185, https://doi.org/10.1109/tmag.1983.1062594.

23. D. C. Jiles and D. L. Atherton, "Theory of Ferromagnetic Hysteresis," *Journal of Magnetism and Magnetic Materials* 61, no. 1–2 (1986): 48–60, https://doi.org/10.1016/0304-8853(86)90066-1.

24. K. Branko, D. Ioan, M. Alenka, and O. Caltun, "Harmonic Analysis and Modelling of Magnetisation Process in Soft Ferromagnetic Materials," *Facta Universitatis – Series: Electronics and Energetics* 30, no. 1 (2017): 121–136, https://doi.org/10.2298/fuee1701121k.

25. Z. Yin, F. Deng, H. Liu, et al., Robust Predictive Voltage Control Strategy for Dual Active Bridge Converter Based on Runge–Kutta (Transactions of China Electrotechnical Society, 1–13), https://doi.org/10.19595/j.cnki.1000-6753.tces.241890.

26. O. L. Jay and I. J. Montijano, "Analysis of Starting Approximations for Implicit Runge-Kutta Methods Using Reverse Method," *Applied Numerical Mathematics* 215 (2025): 1–14, https://doi.org/10.1016/j.apnum.2025.04.007.

27. J. Song, C. Xu, and O. Shishkina, "Finite Difference Method for Turbulent Thermal Convection of Complex Fluids," *Journal of Computational Physics* 525 (2025): 113732, https://doi.org/10.1016/j.jcp.2025.113732.

28. Y. Liu and M. Liu, "Motor Parameter Identification Based on Least Squares and MRAC," *Automotive Electronics* 5 (2025): 126–128, https://doi.org/10.13273/j.cnki.qcdq.2025.05.040.

29. C. Bei, W. Lu, Y. Lu, et al., "Parameter Identification of PMSM Using Recursive Least Squares With Variable Forgetting Factor," *Electronics Technology* (2025): 1–13, https://doi.org/10.16180/j.cnki.issn1007-7820.2025.09.002.

30. R. Wei and Z. Wang, "Structure Optimization of Switched Reluctance Motor Based on PSO Algorithm," *Journal of Henan University of Engineering (Natural Science)* 37, no. 2 (2025): 43–49, https://doi.org/10.16203/j.cnki.41-1397/n.2025.02.009.

31. Z. Chen and Z. Zhang, "Current Stress Optimization of PPDAB Converter Using Improved PSO Algorithm," *Power Electronics Technology* 59, no. 2 (2025): 111–114+118, https://doi.org/10.20222/j.cnki.cn61-1124/tm.2025.02.021.